Review

Brain Perfusion Imaging: How Does It Work and What Should I Use?

CME

Blake E. McGehee, MD,[1]* Jeffrey M. Pollock, MD,[2] and Joseph A. Maldjian, MD[1]

This article is accredited as a journal-based CME activity. If you wish to receive credit for this activity, please refer to the website: www.wileyhealthlearning.com

ACCREDITATION AND DESIGNATION STATEMENT

Blackwell Futura Media Services designates this journal-based CME activity for a maximum of 1 *AMA PRA Category 1 Credit*[TM]. Physicians should only claim credit commensurate with the extent of their participation in the activity.

Blackwell Futura Media Services is accredited by the Accreditation Council for Continuing Medical Education to provide continuing medical education for physicians.

EDUCATIONAL OBJECTIVES

Upon completion of this educational activity, participants will be better able to appraise the different magnetic resonance imaging (MRI) techniques and developments related to cerebral perfusion.

ACTIVITY DISCLOSURES

No commercial support has been accepted related to the development or publication of this activity.

Faculty Disclosures:

The following contributors have no conflicts of interest to disclose:

Editor-in-Chief: C. Leon Partain, MD, PhD

CME Editor: Scott B. Reeder, MD, PhD

CME Committee: Scott Nagle, MD, PhD, Pratik Mukherjee, MD, PhD, Shreyas Vasanawala, MD, PhD, Bonnie Joe, MD, PhD, Tim Leiner, MD, PhD, Sabine Weckbach, MD, Frank Korosec, PhD

Authors: Blake E. McGehee, MD, Jeffrey M. Pollock, MD, and Joseph A. Maldjian, MD

This manuscript underwent peer review in line with the standards of editorial integrity and publication ethics maintained by *Journal of Magnetic Resonance Imaging.* The peer reviewers have no relevant financial relationships. The peer review process for *Journal of Magnetic Resonance Imaging* is double-blinded. As such, the identities of the reviewers are not disclosed in line with the standard accepted practices of medical journal peer review.

Conflicts of interest have been identified and resolved in accordance with Blackwell Futura Media Services's Policy on Activity Disclosure and Conflict of Interest. No relevant financial relationships exist for any individual in control of the content and therefore there were no conflicts to resolve.

INSTRUCTIONS ON RECEIVING CREDIT

For information on applicability and acceptance of CME credit for this activity, please consult your professional licensing board.

This activity is designed to be completed within an hour; physicians should claim only those credits that reflect the time actually spent in the activity. To successfully earn credit, participants must complete the activity during the valid credit period.

Follow these steps to earn credit:

- Log on to www.wileyhealthylearning.com
- Read the target audience, educational objectives, and activity disclosures.
- Read the article in print or online format.
- Reflect on the article.
- Access the CME Exam, and choose the best answer to each question.
- Complete the required evaluation component of the activity.

This activity will be available for CME credit for twelve months following its publication date. At that time, it will be reviewed and potentially updated and extended for an additional period.

In the last 15 years there has been a relative explosion in the number of magnetic resonance imaging (MRI) techniques and developments related to cerebral perfusion. Given the variety of perfusion methods available, it is often difficult to decide which technique would be best for a particular clinical question or patient. In this review article we discuss the more common techniques, review how they are performed, and summarize the optimal technique or techniques for a variety of clinical situations.

ROUTINE CLINICAL PROTOCOLS are in constant flux. The choice of which sequences to include, and equally important, how to perform them, is a difficult one. Implementation in a bustling clinical practice is often a question of practicality, in particular when considering the incorporation of routine functional imaging such as perfusion magnetic resonance imaging (MRI). In this article we review the most widely utilized MRI brain perfusion techniques, how the techniques are performed, when each should or should not be used, and clinical examples of protocol implementation. While this article will at times reference the physical models, sequence details, and other scientific points of perfusion imaging, the goal is to impart a practical understanding of the most widely used MRI perfusion techniques and their use in clinical practice.

All forms of perfusion imaging utilize an intravascular tracer that can be detected in the area of interest. The tracers can be classified as diffusible or nondiffusible based on their interaction with the blood–brain barrier (BBB). For MRI perfusion imaging, gadolinium-based compounds are considered nondiffusible, whereas techniques such as arterial spin labeling (ASL)—that use the native protons in blood water—are considered diffusible.

PERFUSION IMAGING WITH GADOLINIUM

Overview

Brain perfusion imaging performed after the intravenous administration of a gadolinium-chelated contrast agent falls into two categories: dynamic susceptibility-weighted contrast (DSC) and dynamic contrast enhancement (DCE). Both the DSC and DCE techniques are patterned after "tracer kinetic" models of tissue perfusion, which utilize a gadolinium-chelate tracer, track that tracer through the tissue, and then analyze its ingress/egress (1). DSC utilizes the T2* effect of a bolus of gadolinium-chelate—the fundamental observation that the agent causes a transient decrease in signal intensity during initial transit through the vasculature (2–4). DCE, on the other hand, relies on the observation that gadolinium-chelated contrast agents, after the transient T2* effects, cause relative T1 shortening within the blood-pool and within any extravascular space in which the gadolinium-chelate accumulates

because of leakage across the BBB or blood–tumor barrier. These changes can be measured, qualified, quantified, and displayed as regional brain perfusion metrics. Of the gadolinium-based techniques, article focuses primarily on the DSC technique, which currently has greater widespread clinical application than DCE.

Technical Considerations

DSC Perfusion

The standard parameters used in the context of tracer-kinetic models of DSC perfusion imaging are time to peak (TTP), arrival time (AT), cerebral blood volume (CBV), cerebral blood flow (CBF), and mean transit time (MTT). CBV is defined as milliliters of blood per 100 grams of brain tissue (mL blood/100 g). CBF is the volume of blood flowing through a mass of brain tissue over a certain period of time (reported as mL/100 g/min). According to the central volume principle of indicator-dilution theory, CBV, CBF, and MTT are related through the simple equation MTT = CBV/CBF (5,6).

Although confined to the vasculature, the susceptibility effect of a gadolinium-chelate will extend beyond the lumen to the adjacent parenchyma (4). Within a given voxel, the signal intensity will fall as the gadolinium-chelate bolus arrives, which is due to the T2* effects and dependent on the strength of the magnetic field (2). The signal intensity is converted to tissue concentration by Eq. [1]:

$$\text{Tissue concentration}(t) = -k * \log(S(t)/S(0))/TE \quad [1]$$

Here, k is assumed to be constant, S(t) is signal intensity at time (t), S(0) is the signal intensity at time zero, and TE is the echo time of the pulse sequence.

The arrival time is defined as the time from bolus administration to the time the tissue concentration curve begins to rise. The time to peak is the time from bolus administration to peak signal intensity. A simple method to derive relative MTT (rMTT) is the full width at half maximum of the tissue-concentration-over-time curve (or simply, the "tissue concentration curve"). The area under this tissue concentration curve is proportional to CBV (Fig. 1). By integrating the area under the tissue concentration curve, a relative cerebral blood volume metric (rCBV) is defined. This value assumes the T1 effects are negligible, which can be seen in the delayed elevation of the curve baseline. Several techniques including baseline subtraction, model free methods, and gamma variate fit have been used to account for the T1 effects when calculating DSC metrics. The method selected can have a significant influence on the final perfusion measurements (7). The three parameters AT, TTP, and rCBV are the easiest to calculate and the most commonly used clinical perfusion metrics derived from DSC perfusion imaging (5,8–10).

Absolute quantification of DSC perfusion data requires knowledge of the concentration of contrast material in the blood pool. This value, called the arterial input function (AIF), is obtained by measuring the concentration curve of the artery supplying the area of interest. As opposed to relative perfusion data, a quantifiable tissue concentration curve is technically
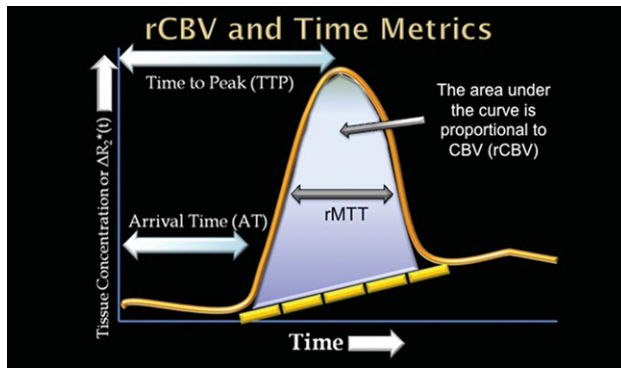
Figure 1. Schematic representation of the time–intensity curve in DSC-MRI perfusion. Tissue concentration of gadolinium-chelate is on the Y-axis and time on the X-axis. Simplistically, the area under the curve is proportional to relative cerebral blood volume within the voxel of interest. The arrival and peak of the signal change equates to arrival time (AT) and time to peak (TTP), respectively, which are the most commonly used transit parameters. The full width at half maximum concentration is the relative mean transit time (rMTT). [Color figure can be viewed in the online issue, which is available at wileyonlinelibrary.com.]

derived using the AIF, the CBF, and the tissue residue function, R(t), which is the amount of contrast remaining in the tissues at time (t). A mathematical process called deconvolution can extract the CBF and R(t) from the tissue concentration curve if the AIF is known. CBV is then calculated, which is equal to the integral of the tissue concentration curve divided by the integral of the AIF curve. MTT is easily derived once CBV and CBF have been measured, as MTT = CBV/CBF (MTT also equals the area under the R(t) curve). The challenges associated with absolute quantification of perfusion metrics from DSC perfusion imaging are numerous. The final values obtained are highly dependent on the AIF measurement. There are inherent difficulties with this measurement. The AIF is related to cardiac output, vascular tone, which artery is selected, which arm was injected and, most significantly, partial volume effects related to the small size and volume averaging of the intracranial vessels (10,11). The partial volume effects act in a nonlinear fashion, compromising perfusion quantitation, especially at the longer echo times typically used for clinical imaging (12). There are many deconvolution models, but no single method has been universally accepted to date. Furthermore, there is no uniformity among methods used in practice, most of which have not been thoroughly validated (13,14). As such, the difficultly in performing accurate and reproducible absolute perfusion quantification using DSC techniques is one of the primary weaknesses of this method, which is an important problem with clinical implications. Without accurate quantification, for example, one cannot compare perfusion data in the same patient over time, especially when searching for subtle change or global perfusion patterns. In general clinical practice, the simple solution is to use the AT, TTP, and rCBV maps. These parameters provide relevant, reliable data about the pathologic process being evaluated.

The methods described above assume that the gadolinium remains an intravascular tracer throughout image acquisition. If the BBB is dysfunctional or "leaky," the DSC data can be compromised. This relates to the relative shortening of the T1 of water in the presence of parenchymal contrast extravasation, which counteracts or mutes the T2* effect/signal intensity decrease (2,15). Recent comparative studies have shown that a "preload" of gadolinium-chelate, given before the actual bolus dose for DSC data acquisition, can reduce the deleterious impact of a leaky BBB on the perfusion data (7). The preload reduces the T1 leakage effects by saturating the "leaky" tissues with gadolinium-chelate, thereby dampening the T1 shortening effects of the main bolus during DSC-MRI acquisition (16). At our institution, a "preload" bolus of gadolinium-chelate is routinely administered prior to DSC perfusion imaging.

DCE Perfusion

DSC MRI remains the clinical standard among perfusion techniques utilizing a gadolinium-chelate, but errors are inherently introduced into the data processing for a variety of reasons, including the difference in relaxivity between tissue and blood pool (17) and the problems inherent in BBB breakdown, as discussed above. For these reasons and others, alternative methods of gadolinium-chelate perfusion imaging have been advanced, chiefly DCE-MRI. DCE-MRI perfusion uses metrics to describe the permeability of the BBB and the relationship to the extracellular extravascular space (EES). The same leakage that confounds the DSC perfusion is measured with DCE using a dynamic T1-weighted sequence. The acquisition time course is often over several minutes for DCE, while DSC is about 60 seconds in length. This time allows for measurement of the wash-in and wash-out of the contrast material in the EES. There are several methods for image interpretation. The simplest method is to examine the signal intensity curves over time for a region of interest. The rate or slope of the wash-in and wash-out curve for multiple regions of interest can be visually assessed. This type of assessment is valuable for distinguishing tumors (rapid curve rise) from radiation necrosis (slow curve rise). Semiquantitative methods can also be used and parametric maps can be easily created showing the slope of the wash-in and wash-out curves, maximal enhancement, and arrival time. Additional quantitative methods can also be performed by integrating the initial area under the DCE tissue concentration curve (IAUCC). This metric has been shown to be similar to the more advanced DCE parameters; however, it also reflects multiple physiologic processes including permeability, volume of the EES, and blood flow (11,18). More advanced processing involves use of T1 maps, a vascular input function (much like the AIF in DSC-MRI), and complex pharmacokinetic models. This later method of post-processing provides the metrics k^{trans} (the transfer coefficient between the plasma and EES that reflects permeability of the BBB), v_p or fractional plasma volume, and v_e or fractional volume of the EES (11). These variables are related by Eq. [2]:

$$v_e(dC_1/dt) = k^{trans}(C_p - C_1) \qquad [2]$$

C_1 is the measured tissue concentration, and C_p is the plasma concentration acquired from the AIF.
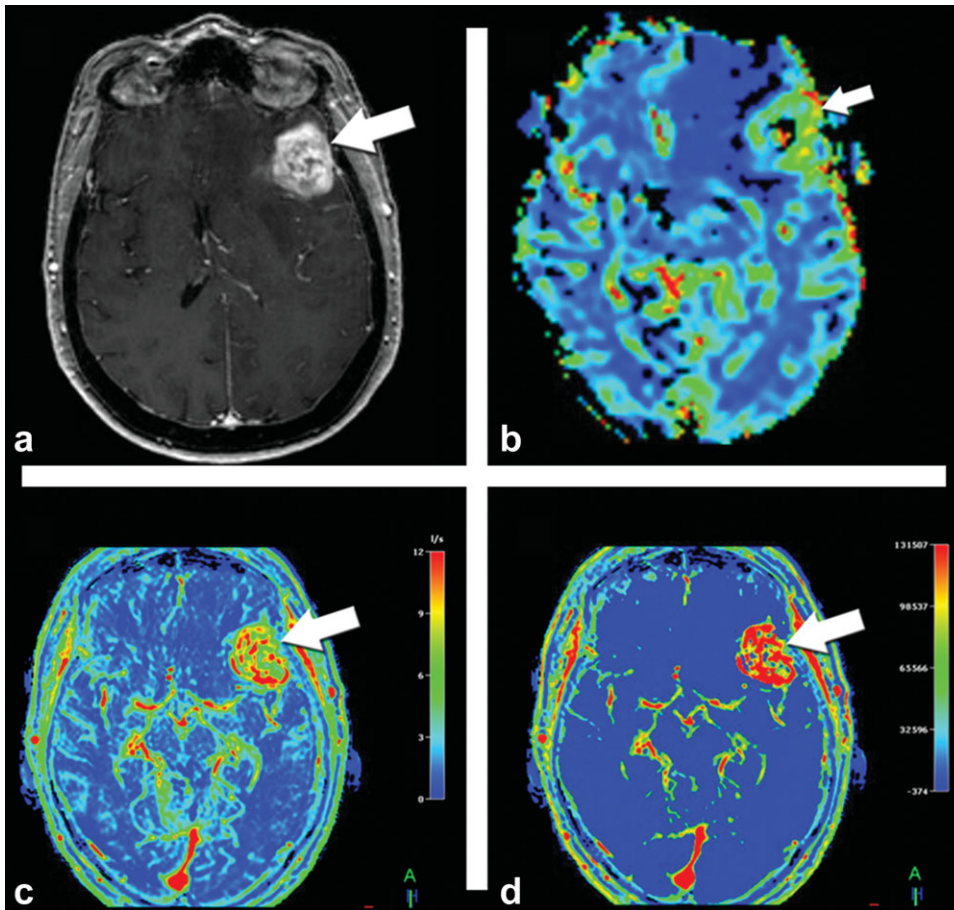
Figure 2. Glioblastoma multiforme (GBM). **a:** An avidly enhancing mass is identified in the inferior left frontal lobe (arrow). **b:** DSC perfusion shows a high rCBV (arrow) that measured 2.23 compared to the contralateral white matter. **c:** Wash-in perfusion map derived from DCE shows a rapid rate of wash-in of the mass (arrow). **d:** Initial area under the tissue concentration curve (IAUGC) obtained from the DCE data shows a very high value (arrow). This parameter reflects permeability, volume of the EES, and CBF. [Color figure can be viewed in the online issue, which is available at wileyonlinelibrary.com.]

Quantitative DCE perfusion suffers from the same need and limitations of the AIF as DSC perfusion. One difficulty in this technique is that the T1 changes are an order of magnitude less than the T2* effects measured with DSC (17). But one of the main limitations of this technique, and perhaps the reason it has not yet achieved widespread clinical use, is the difficulty in the DCE tracer kinetic model. Early work with DCE-MRI utilized a "one-compartment" model, which does not allow CBV quantification (19,20). Further, this model loses validity in the setting of a leaky BBB. Recent studies have evaluated CBV and CBF quantification by DCE-MRI using "two compartment" models (21,22). Regardless, the DCE model selected can have significant effects on the final values of k^{trans} and v_e. Furthermore, the AIF selected can also have significant effects on the final metric. These inherent challenges make it difficult, if not impossible, to compare k^{trans} values between different models, publications, and patients. Because the optimum modeling of DCE-MRI data is still a "moving target," major MRI vendors have been slow to offer the software necessary for clinical quantitative data analysis. Likely, for this reason more than any other, it remains secondary to DSC-MRI and arterial spin label imaging (which is discussed in detail below). Indeed, the current clinical roles for DCE are primarily confined to the characterization of tumors (Fig. 2), evaluation of recurrent tumor versus radiation necrosis, and changes in tumor microvasculature in response to therapy. Multi-institutional efforts such as the Quantitative Imaging Biomarkers Alliance (QIBA)—sponsored by the Radiological Society of North America—are currently under way to establish reference measures and best practices that could serve as a basis for more widespread clinical implementation.

PERFUSION IMAGING WITHOUT GADOLINIUM

Overview

MRI perfusion imaging without the use of gadolinium-chelate contrast agents is performed through "spin tagging," more commonly called arterial spin labeling (ASL). In this method, diffusible and magnetically labeled protons within blood water flow into the brain, where they are imaged. This technique was developed and conceptualized almost 20 years ago, but has only recently gained clinical feasibility (23). ASL has some intrinsic advantages over DSC and DCE perfusion imaging. ASL requires no intravenous contrast, thus avoiding the risk of nephrogenic systemic fibrosis (24). Moreover, intravenous access is not necessary, which can often be the source of clinical delays, particularly in the pediatric setting. Quantified CBF can be obtained by ASL methods (25). Furthermore, absolute CBF obtained with ASL compares favorably to the "gold-standard" technique of positron emission tomography (PET) (26). However, ASL provides low image signal-to-noise ratio (SNR), as signal is from endogenous contrast (blood), which has a small fraction in

the tissue (≈1%), most ASL implementations currently provide CBF alone, and sensitivity to transit delay, delivery time from the location of tagging to the target tissue, often hinders accurate quantification of CBF especially in clinical applications.

Technical Considerations

Arterial Spin Labeling

ASL is performed in a two-step manner with a preparation and acquisition phase. In the preparation phase, blood flowing toward the brain parenchyma is "labeled" by a radiofrequency (RF) pulse; this is performed in the "tagging plane." Next, the labeled blood flows to the brain, sometimes waiting a predetermined time known as the "postlabeling delay" before the final phase. In the acquisition phase, a series of slices within the brain are imaged both with and without (control) the label. This is performed in the "imaging plane."

Manipulating the parameters of the preparatory phase has led to nuances within the general method. There are four basic varieties, known as pulsed arterial spin label imaging (PASL), continuous arterial spin label imaging (CASL), pseudocontinuous arterial spin label imaging (PCASL), and velocity-selective arterial spin label imaging (VS-ASL). Each differs in the technique utilized to deliver the magnetic tag to the inflowing blood. PASL uses short RF pulses to invert a thick slab of spins proximal to the imaging plane. CASL uses long and uninterrupted RF pulses to invert a narrow slice of spins adjacent to the imaging plane. As the name implies, this is done in a continuous manner while the spins flow through the tagging plane into the imaging plane. Although this results in higher perfusion sensitivity than with PASL, the continuous RF pulse deposits large amounts of energy into the patient, which can potentially exceed the specific absorption rate (SAR) limits established by the Food and Drug Administration (27). Further, the hardware to generate a continuous pulse is not available on many commercial MR scanners and CASL often requires separate labeling and imaging coils to circumvent some of the SAR and magnetization transfer limitations (28). In response to these limitations, PCASL was developed to mimic the tagging mechanism of CASL without the inherent drawbacks. This is accomplished by rapidly repeating gradient and RF pulses to attain near-continuous labeling with high efficiency but without the hardware requirements and magnetization transfer effects of CASL (29). Although promising, PCASL is not yet widely available. While PASL, CASL, and PCASL perform tagging based on location of the flowing blood, VS-ASL saturates blood flowing within a specified velocity range, and in this manner provides contrast for perfusion imaging. Since the tagging is applied at a location proximal to the imaging plane, it is postulated that VS-ASL has less significant transit delay effects with greater uniformity. It may have more utility in the context of slow flow and/or collateral flow conditions (30,31). However, the low SNR of ASL is exacerbated in VS-ASL, since spins are labeled by saturation pulses instead of inversion pulses as in the other ASL methods.

To date, the PASL technique is the most widely available and is used at our institution. Ideally, all of the energy imparted on protons in the tagging plane will be deposited into the parenchyma of the imaging plane prior to the initiation of the imaging acquisitions. This does not always happen, and some of the tag will remain in the intravascular space. If imaged and quantified, this lingering intravascular tag can lead to inaccurate perfusion data. The removal of the intravascular label can be facilitated by the utilization of bipolar "crusher" gradients, which essentially suppress the signal of moving spins, ie, those that remain in the intravascular space. Lack of a crusher gradient makes quantification difficult because the intravascular tag can artificially inflate tissue perfusion results. Beyond quantification, the presence or absence of crusher gradient use in pathologic conditions, such as slow flow situations, significantly affects the appearance of pathology. If a crusher gradient is used in slow flow situations, there will be a large apparent perfusion defect because much of the tag does not reach the parenchyma. The crusher gradient will null this signal and the final image appears more like a transit time map, and no longer reflects actual CBF in the area of slow flow. Thus, in a slow flow scenario with a crusher gradient, perfusion is underestimated. In the same situation, without a crusher gradient, the slow flow region will have high linear intravascular signal and CBF could be overestimated. The disadvantage of crusher gradients is that they decrease the overall signal by suppressing the intravascular components (32). In some situations, however, it can be advantageous to identify the presence of significant intravascular signal, indicating a slow flow condition. Therefore, the application of crusher gradients is not uniformly performed.

Between the preparatory phase and acquisition phase of ASL is the postlabeling delay (PLD), known as the inversion time in PASL imaging. This is an extremely important parameter in the performance of ASL. The benefits of a brief PLD include shorter scan time and a relatively large amount of nondecayed signal. However, with a short PLD the tagged blood may not have had time to reach the parenchyma of the imaging plane and the perfusion signal is artificially low. Further, there is less time for the label to diffuse into the tissue, placing a greater need on crusher gradients, which, if used, result in an image that underestimates perfusion (33). The benefits of a long PLD include greater potential signal within the imaging plane and more accurate depiction of cerebral perfusion. Drawbacks include a relatively small amount of signal remaining after T1 decay and increased total scan length, which notably also increases the likelihood of motion artifact. As with most MRI parameters, there is no perfect value for the PLD, which ultimately depends on the patient population being imaged. Familiarity with normal age-related changes in ASL perfusion data may be helpful in choosing the appropriate PLD and with scan interpretation (19,33,34).

Following the delay, the data are acquired, conventionally with echo-planar imaging (EPI) sequences, because of the fast acquisition and simple reconstruction. During acquisition, suppression of the static signal of normal tissues in the imaging plane is important to improve SNR (35). Also during acquisition,

numerous label/control pairs are typically acquired (eg, 60 pairs for the PASL technique). With appropriate crusher gradient application, the change in signal between the label/control pairs represents the perfusion, but the signal change is small (1%–2%). Increasing the number of label/control pairs improves SNR, but adds time to scan length. The signal difference is influenced by a variety of factors, including the T1 of blood and brain parenchyma, and the time necessary for the blood to travel from the tagging plane to the imaging plane, during which signal decay occurs. Once acquired, the data are processed, which consists of motion correction, subtraction of alternating label/control pairs, tissue segmentation, and CBF quantification. The CBF is calculated in PASL using Eq. [3]:

$$f = \frac{\Delta M(TI_2)}{2M_{0,blood}\,\alpha\,TI_1\,q\left(T_{1,tissue}, T_{1,blood}, f, \lambda, TI_2\right)}\,e^{\left(\frac{TI_2}{T_{1,blood}}\right)}$$

[3]

Here, f is the cerebral blood flow, $\Delta M(TI_2)$ is the difference in the signal intensity between the control and label images, $M_{0,blood}$ is the equilibrium magnetization of blood, α is the tagging efficiency, TI_1 is the time duration of the tagging bolus, λ is the blood-brain coefficient, TI_2 is the inversion time of each slice, and $T_{1,blood}$ is the longitudinal relaxation time of blood; q is a correction factor that accounts for the difference between the T1 of blood and the brain tissue (36).

At our institution, the grayscale CBF maps are converted to color Joint Photographic Expert Group (jpeg) images using a standardized color perfusion scale, with both grayscale and color jpeg images sent to the picture archiving and communication system (PACS). The standardized color jpeg CBF maps allow for rapid clinical interpretation and comparison across timepoints and between patients, whereas the grayscale images allow localization with conventional imaging sequences and conventional manipulation of brightness and contrast. As for vendor-supplied product implementations, no current standardization of color has yet been determined. Greater detail can be found in several recent publications for improving PASL images with data filtering (37) and clinical implementation (38).

The ability to acquire ASL perfusion data, and the software to process it, are commonplace now among major MRI vendors. Currently, most vendors utilize the PASL technique, which may soon be replaced by PCASL. Our PASL technique utilizes quantitative imaging of perfusion and a single subtraction with thin section TI_1 periodic saturation (QUIPSS II TIPS, OR Q2TIPS) (36) with a flow-sensitive alternating inversion recovery (FAIR) sequence (39). The Q2TIPS-FAIR sequence incorporates saturation pulses, which convert a spatially tagged bolus into a temporal bolus, allowing quantification. By combining Q2TIPS-FAIR with EPI for localization, we routinely obtain 11 sections consisting of 60 label/control pairs. The scan time is ≈6 minutes 30 seconds. At our institution, the pulses saturate a 2-cm slab of tissue, which is spaced 1 cm from the first slice of the imaging plane. Crusher gradients are utilized to suppress intraarterial spins from tagging performed earlier

in the sequence, which may not have dissipated during subsequent rounds of tagging (25,32).

Clinical Protocol

Our clinical protocols were developed primarily on a General Electric platform, but comparable techniques are available through other major vendors. In essence, on all routine brains we acquire perfusion data utilizing all three techniques outlined above. Once implemented, this is rather simple to perform. ASL does not use gadolinium-chelate contrast and the T1 shortening caused by gadolinium destroys the ASL signal. Therefore, ASL is the first perfusion sequence acquired. Both DSC and DCE techniques require gadolinium, but are largely unrelated in the mechanism whereby imaging contrast is provided. We take advantage of the need to preload for the DSC technique and acquire the DCE portion of the exam first, using 1/3 of the normal weight-based dose of gadolinium. The DCE acquisition serves as the preload for the subsequent DSC exam, which is obtained with the remaining weight-based dose of gadolinium. In the context of the entire scan, both conventional and perfusion scanning, the progression of sequences is the following: localizer, precontrast conventional structural imaging (including diffusion-weighted imaging/diffusion tensor imaging), PASL, DCE, DSC, and finally postcontrast conventional imaging. All sequences can be performed at 1.5T or 3T field strength and can benefit from multichannel coils with acceleration technologies. More details regarding each perfusion protocol are further discussed below.

ASL

Q2TIPS-FAIR sequence for labeling with EPI acquisition: TE, 28 msec; TI_1, 800 msec; TI_{1s}, 1200 msec; TI_2, 2000 msec; TR, 3000 msec; receiver bandwidth, 62.5 kHz; flip angle, 90°; field of view (FOV) 24 × 18 cm; matrix 64 (frequency) × 48 (phase); 11 sections, 8 mm thickness, 0 gap. A PASL T1 map is acquired after the Q2TIPS-FAIR/EPI sequence to aid in quantification.

DCE

The volume of contrast used to gather the DCE data also serves as the DSC preload. Much work has been done to determine the optimum preload technique (7,16). We keep the total gadolinium-chelate administered dose at the standard 0.1 mmol/kg and use 1/3 of this total dose for the DCE acquisition. This is power-injected at a rate of 4–5 cc/sec. Ultrafast gradient echo sequence (3D SPGR FAST), multiphase with asset calibration: TE, minimum; receiver bandwidth, 25 kHz; flip angle, 20°; FOV 24 cm; matrix 256 (frequency) × 192 (phase); 10 sections, 7 mm thickness. Typically, there are ≈30 phases with 12 slices per phase. Total scan length is ≈3 minutes 30 seconds.

DSC

The remaining calculated gadolinium dose (2/3 of 0.1 mmol/kg) is power-injected at a rate of 4–5 cc/sec. Gradient recalled EPI sequence (2D GE, EPI), multiphase: TE, 54 msec; TR, 2000 msec; flip angle, 35°; FOV 24 cm; matrix, 256 × 256. Slice thickness can
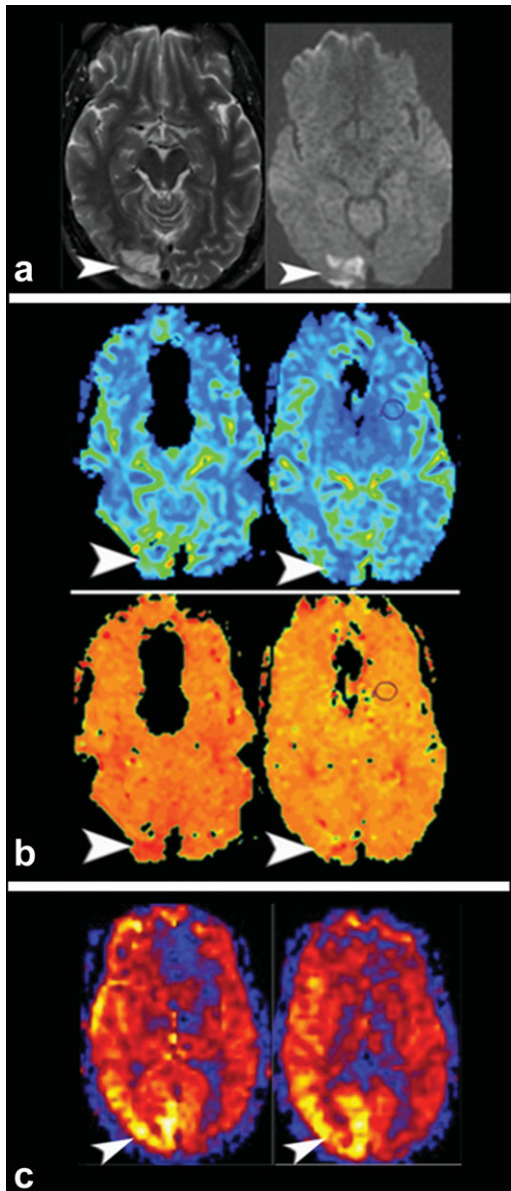
Figure 3. a: A subacute infarct is apparent within the right occipital lobe, evidenced by increased cortical T2 signal intensity and restricted diffusion (arrowheads). **b:** With DSC, the lesion is difficult to detect on both rCBV (top row) and TTP (bottom row) maps (arrowheads). **c:** The ASL CBF map clearly depicts the subacute infarct, exhibiting focal hyperperfusion, or luxury reperfusion (arrowheads). [Color figure can be viewed in the online issue, which is available at wileyonlinelibrary.com.]

vary, but is typically 5–7 mm with 16 axial slices per perfusion dataset. A total of 60 phases are acquired with 16 slices, and the typical dataset contains ≈960 images. Total scan length is ≈1 minute 45 seconds (at 1.5T). Scan length is marginally longer (2 minutes) at 3T, due to a slightly longer TR.

Clinical Use

Screening

Because the techniques differ vastly and the physiologic depictions of perfusion are unique for DSC MRI

(typically TTP and rCBV) versus ASL (quantitative CBF), there are situations when one is favored over the other. In our general experience, without a priori knowledge of lesion location, pathology tends to be more conspicuous on ASL CBF maps than DSC maps (Fig. 3). Further, because DSC provides relative data, there is variability among perfusion maps over time for the same patient, in spite of identical scanning techniques. This can lead to additional issues with lesion detection and/or characterization (Fig. 4). Finally, just as there can be variability over time for DSC perfusion data, there is often slice-to-slice variability within the same scan, particularly on TTP maps. For these reasons, and because gadolinium is not needed, we prefer ASL for screening purposes. While we have constructed our own automated system for ASL processing to aid with research, major MRI vendors now provide "turn-key" solutions for ASL utilization in everyday clinical use, making it a viable option for incorporation into routine clinical scanning.
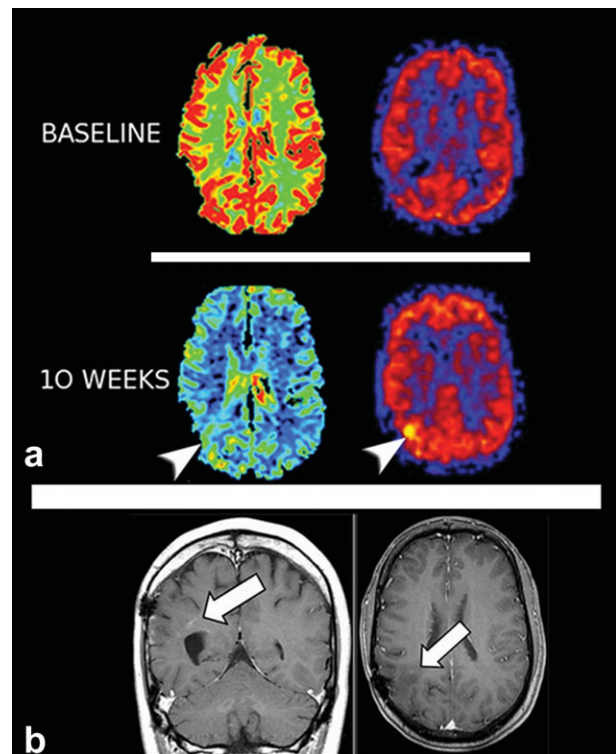

Figure 4. This patient is status post high-grade glioma resection within the right parieto-occipital region, with several stable follow-up exams. **a:** Representative images from baseline (top row) and roughly 10 weeks later (bottom row). The images at left are DSC-MRI rCBV maps, and the images at right are ASL CBF maps. In spite of identical scan parameters, the DSC-MRI data (images at left) appear vastly different, which is the result of scaling and the relative nature of DSC. In contrast, the ASL CBF maps (images at right) exhibit constancy across exams, allowing for comparison of perfusion data over time. A focus of hypervascularity is easily identified (arrowheads) with ASL. **b:** A subtle focus of enhancement, which could easily be overlooked without a focused search on behalf of the ASL data, is present on postcontrast T1 imaging at the 10-week scan. Subsequent scans confirmed recurrence. [Color figure can be viewed in the online issue, which is available at wileyonlinelibrary.com.]
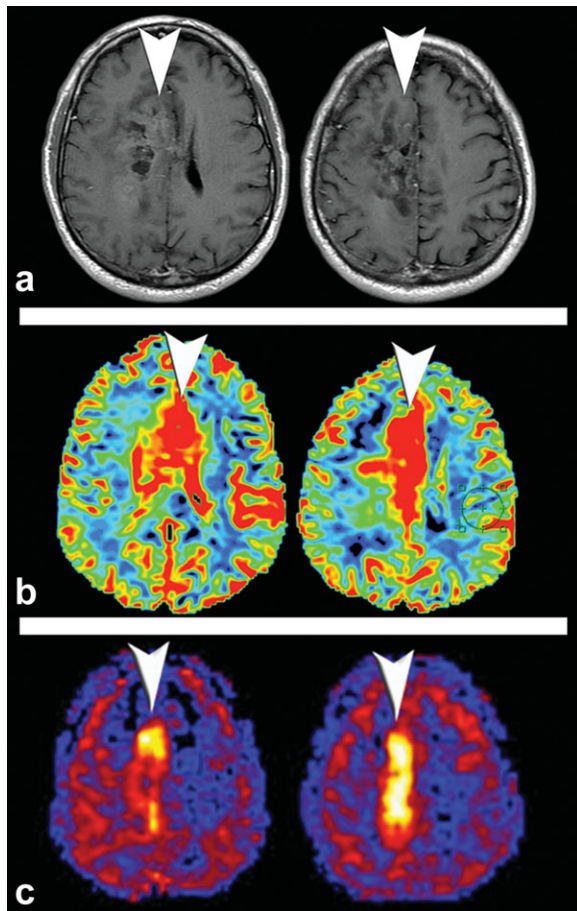
Figure 5. a: On T1 postcontrast imaging, the tumor within the corpus callosum is primarily nonenhancing (arrowheads). Hyperperfusion on both DSC perfusion rCBV map **(b)** and ASL perfusion CBF map **(c)** (arrowheads) is concerning for high-grade histology, confirmed as World Health Organization (WHO) grade III anaplastic astrocytoma after resection.

Tumor Imaging

Cerebral perfusion estimates based on DSC and ASL data have proven clinically useful regarding tumor grade, biopsy guidance, recurrence versus radiation necrosis, response to treatment, and prognosis. It is well established that there is a direct correlation between angiogenesis and glioma tumor grade (40–42). It has further been demonstrated that DSC-MRI is capable of identifying regions of hypervascularity on rCBV maps that correlate with tumoral areas of dense angiogenesis, and thus can predict tumor grade (43–45). Some authors investigating gliomas have normalized rCBV as a ratio between a region of interest placed on the mass and the contralateral normal white matter. It is nonetheless a reflection of rCBV and remains the most useful DSC metric when imaging gliomas (9,46). Studies indicate that ASL techniques are likewise capable of identifying increased perfusion in higher-grade gliomas (47,48). The newer PCASL techniques may in fact be better than DSC-MRI (49). Regardless, angiogenesis, and therefore higher histologic grades of tumor, manifest as increased rCBV or CBF on maps generated with

either technique. It is our experience that this can have significant clinical impact by several means. Regions of tumoral hyperperfusion, although it may seem intuitive, do not necessarily enhance following contrast administration on conventional postcontrast T1 imaging, a so-called "perfusion-enhancement mismatch." A disruption in the BBB is obligatory for enhancement, but not for hyperperfusion. This becomes important in several scenarios, most commonly that of a glioma suspected to be low-grade because of little or no contrast enhancement, or infiltrating tumors such as gliomatosis cerebri (50). If such a tumor has hyperperfusion by either DSC or ASL technique, the histologic grade is likely higher than that suggested by anatomic imaging (Fig. 5). This prebiopsy or presurgical suspicion of a high-grade neoplasm may certainly affect treatment planning. Moreover, for biopsy planning the surgeon must consider foci of hyperperfusion because misgrading a tumor by undersampling can result in incorrect tumor
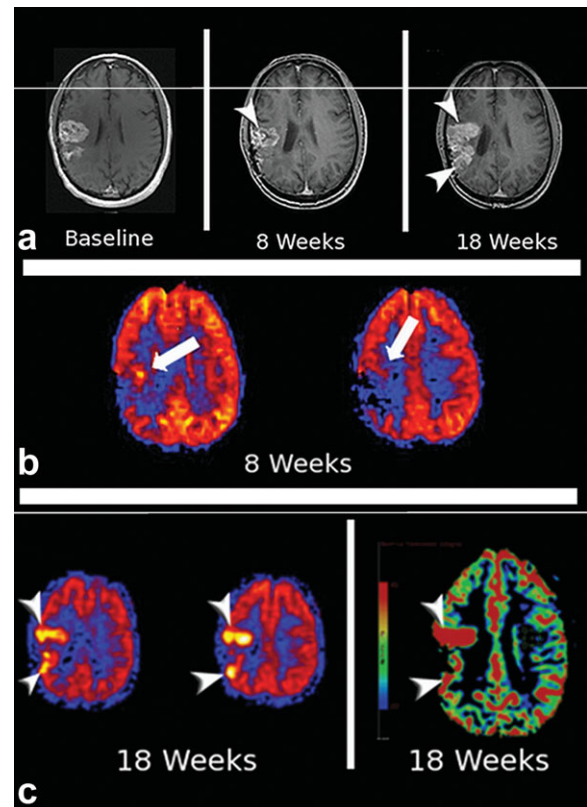

Figure 6. This patient is status-postresection of WHO grade IV GBM, also treated with chemotherapy and radiation. **a:** Sequential postcontrast T1 images at "time zero" (left), 8 weeks (center), and 18 weeks (right). Comparison of the residual enhancing tissue between time zero and 8 weeks is reassuring, as the enhancement has regressed (arrowhead). **b:** ASL CBF map at 8 weeks demonstrates a small focus of increased perfusion within the anteromedial aspect of the tumor bed (arrows). Based on this, recurrence was suggested in spite of decreased enhancement. DSC MRI perfusion was not performed at 8 weeks. **c:** At 18 weeks the ASL hyperperfusion (arrowheads left) and DSC increased rCBV (arrowheads right), along with the solid mass-like enhancement at 18 weeks of image A (arrowheads), confirm recurrence.
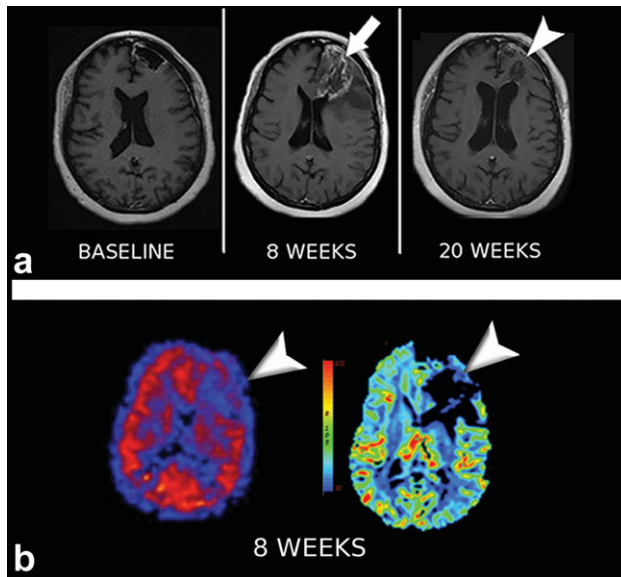
Figure 7. A 52-year-old woman with left frontal lobe GBM (WHO grade IV), status postresection and treatment with chemotherapy and radiation. **a:** Postcontrast axial T1 imaging of the resection cavity at baseline (left), 8 weeks later (middle) with new irregular enhancement and surrounding edema (arrows), and 20 weeks (right) with interval regression of enhancement (arrowhead) confirming the diagnosis of pseudoprogression. **b:** CBF map from ASL MRI perfusion (left) and rCBV map from DSC MRI perfusion imaging (right) both obtained at 8 weeks from baseline, demonstrate hypoperfusion (arrowheads) in the left frontal lobe, including those areas of new enhancement. Perfusion data strongly suggests pseudoprogression, and the patient was managed conservatively with short interval follow-up. Without perfusion data, this patient might have been subjected to unnecessary treatments.
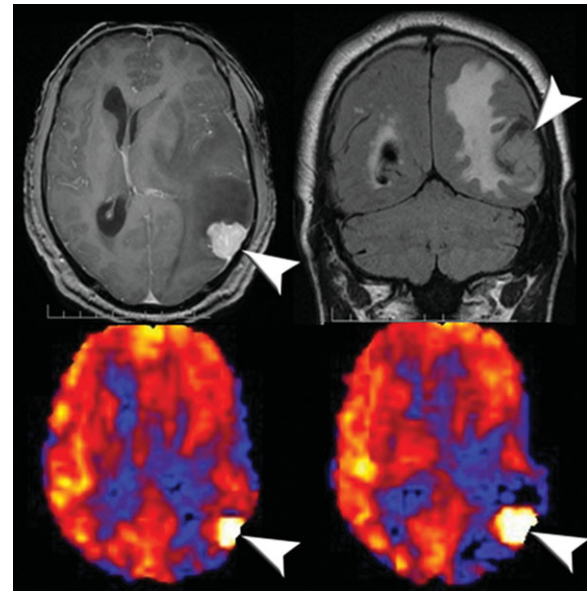

Figure 8. Axial T1 postcontrast (top let), coronal T2 FLAIR (top right), and CBF map images from PASL perfusion (bottom) demonstrate an avidly enhancing, focally hyperperfused extra-axial mass, causing significant edema and mass effect throughout the left hemisphere (arrowheads). After resection, a meningioma was confirmed.

grade, incorrect treatment, and poor patient outcomes. In the patient's interest, it is also incumbent upon the radiologist to ensure radiologic-pathologic correlation in such scenarios. If the biopsy yields a low-grade tumor in the context of a focal hyperperfusion pattern, this should be considered a "discordant" finding to some degree and investigated. These issues

Figure 9. Toxoplasmosis (top row) versus lymphoma (bottom row) in immune-compromised patients. Axial T2, axial T1 postcontrast, DSC perfusion TTP map, DSC perfusion rCBV map, ASL perfusion CBF map, and PET (from left to right) demonstrate the typical findings in toxoplasmosis—a ring enhancing lesion which is hypoperfused and hypometabolic on PET (arrows). In distinction, the right temporal lobe lymphoma is more solidly enhancing, hyperperfused, and hypermetabolic on PET (arrowheads).

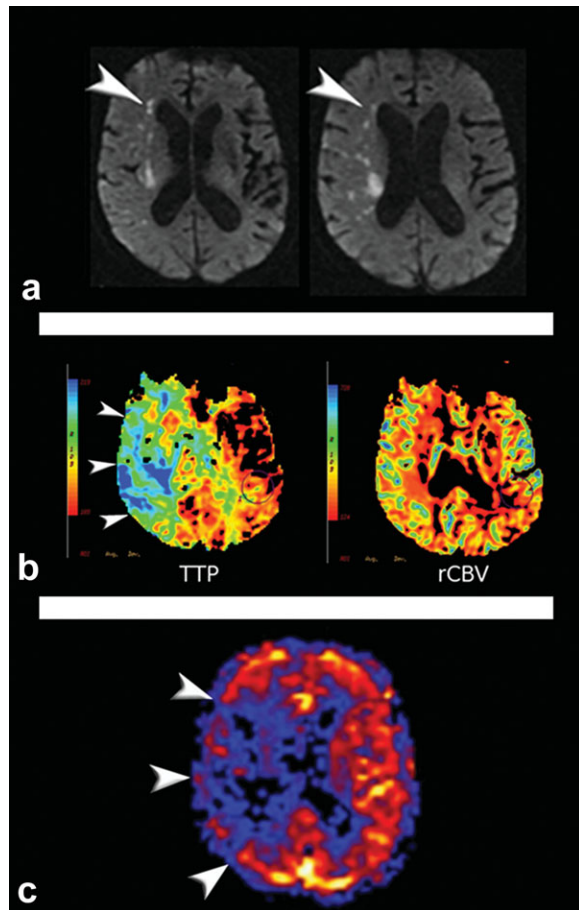**Figure 10.** A male patient presented with acute stroke symptoms. **a:** Axial diffusion-weighted images show scattered punctate areas of infarct within the right middle cerebral artery (MCA) territory (arrowheads). **b:** DSC-MRI perfusion shows increased TTP throughout the right MCA territory (arrowheads) with preserved rCBV. The "diffusion-perfusion" mismatch is consistent with penumbra. As discussed, in cases of extremely slow flow, ASL CBF perfusion maps approximate transit times. **c:** The ASL image (arrowheads) mimics the TTP map from DSC perfusion.

are routinely discussed in our multidisciplinary neuro-oncology conferences.

Note should be made that oligodendrogliomas have been observed to violate the principles outlined above, at times demonstrating a focal hyperperfusion pattern yet remaining low-grade histologically (51). Other non-glial tumors may remain low-grade histologically, but with a focal hyperperfusion pattern, including meningiomas and hemangioblatomas.

While the preceding discussion focuses more on "preoperative/pretreatment" issues, MRI perfusion has also gained acceptance and utility in postsurgical/treatment follow-up. The issue of disease progression versus radiation necrosis is a common dilemma in neuro-oncology. Although vastly different in terms of prognosis and treatment, the entities can be shockingly similar on anatomical imaging, demonstrating areas of patchy and irregular enhancement surrounded by T1 and T2 prolongation. Recurrent high-grade glioma is typically hyperperfused, whereas radiation necrosis is

typically hypoperfused (Fig. 6). In this context, however, DSC-MRI can yield mixed results and some advocate the use of DCE perfusion data to discriminate tumor recurrence/progression from radiation necrosis (11). Perfusion imaging has also proved useful with the entity of "pseudoprogression," a concept that can also confound follow-up scans. Pseudoprogression describes an imaging phenomenon by which the enhancing portions of a known central nervous system (CNS) neoplasm (typically glial) enlarge over successive posttreatment scans. Continued follow-up will then demonstrate the subsequent involution of the enhancing tissue, which radiographically represents a response to treatment. The phase of this process whereby the enhancement enlarges was thus aptly named pseudoprogression. As with radiation necrosis, tumoral pseudoprogression is typically hypoperfused with DSC or ASL. This phenomenon is becoming increasingly more common with the advent of newer combined treatment therapies for glial neoplasms (Fig. 7) (52,53).

Regarding perfusion imaging of extra-axial masses, in particular dural-based lesions such as meningiomas, ASL techniques may seem to have an advantage over DSC. As a BBB is not associated with extra-axial masses, there is potential for the T1 shortening effects of gadolinium-chelate to further mask the T2* effect with DSC-MRI, thus underestimating rCBV of these masses using flip angles of 90°. More recently, studies in animal models have shown that tissues that are considered more leaky (or that lack a BBB) can also affect ASL and although ASL is considered a freely diffusible tracer method, there is still some dependence on an intact BBB for accurate ASL quantification (54). Currently, in extra-axial masses such as meningiomas the ASL signal is thought to diffuse freely into the mass, effectively overestimating CBF. This overestimation has some benefits, because the resulting high contrast between meningiomas and normal tissue make them very easy to detect with ASL (Fig. 8). Perfusion imaging has proven useful in the assessment of immune-compromised patients with enhancing intracranial masses. In this scenario, the question is often one of CNS lymphoma versus opportunistic infection, most commonly toxoplasmosis. While nuclear medicine techniques address this question as well, these patients often present with focal neurologic signs or altered mental status and are therefore in need of MRI brain imaging, not addressed by brain PET or single photon emission computed tomography (SPECT). MR perfusion affords the ability to diagnose CNS lymphoma or toxoplasmosis without the need for additional brain PET or SPECT. Small studies to date validate the observation that CNS lymphoma is hyperperfused and toxoplasmosis is hypoperfused (55). This has similarly been our experience with both DSC and ASL techniques (Fig. 9) (32).

In summary, low-grade solid and cystic glial neoplasms are typically hypoperfused. High-grade glial neoplasms (or foci of high-grade histology within a glial neoplasm) are typically hyperperfused. These hyperperfused areas should be targeted with biopsy. Solid metastases are often hyperperfused, as are some nonglial lower-grade neoplasms, eg, meningioma and hemangioblastoma. Extra-axial tumor perfusion is
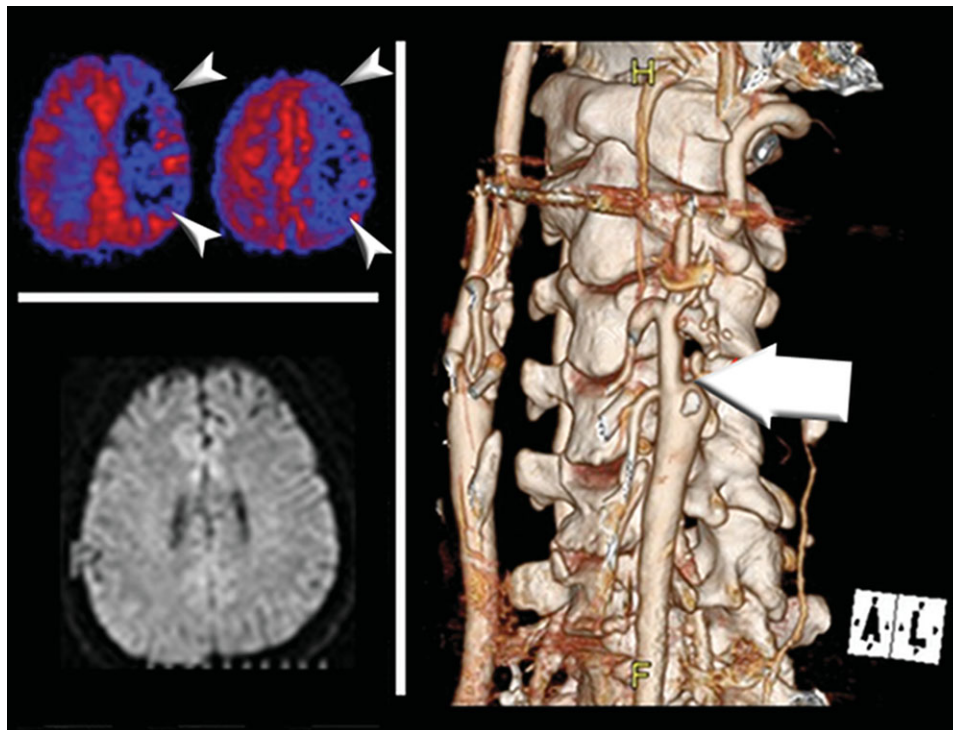
Figure 11. A 49-year-old man presented with intermittent right-hand numbness. Color images from ASL MRI perfusion CBF map (top left) demonstrate hypoperfusion within the left MCA territory (arrowheads) without a corresponding abnormality on diffusion-weighted imaging (bottom left). Therefore, this is a "territory at risk." CTA was recommended, and 3D color surface rendered reformat (right) demonstrates an abrupt vessel cutoff of the left internal carotid artery (arrow). Brain CTA (not pictured) demonstrated an intact Circle of Willis, thus preventing infarction at the time of these exams. [Color figure can be viewed in the online issue, which is available at wileyonlinelibrary.com.]

variable, but often hyperperfused, and can be underestimated with DSC-MRI and overestimated by ASL. In an ideal example, radiation necrosis and pseudoprogression are both hypoperfused on DSC and ASL and can be distinguished on DCE wash-in rates. In general, DSC and ASL are comparable methods for perfusion evaluation of tumors and tumor follow-up. As oncology patients often have comorbidities, and renal dysfunction is a common one, the option to perform the nongadolinium ASL techniques is an advantage in this setting.

Vascular Imaging

MR perfusion imaging of the brain has proven useful in the assessment of various vascular disturbances, mainly infarct, infarct penumbra and/or territory at risk, and in autoregulatory disturbances.

"Stroke protocol" computed tomography (CT) imaging of the brain remains the first-line evaluation in the setting of suspected acute stroke at most institutions, for various reasons. The limitations of noncontrast CT (NCCT) brain scanning alone are well known, including underrecognition of infarct, inability to identify penumbra or tissue at risk, and the low positive predictive value of NCCT regarding those patients who will benefit from systemic or catheter-directed interventions. Stroke mimics are also underrecognized by NCCT. For these reasons, CT perfusion and CT angiography (CTA) are now commonly included in stroke protocols. However, MRI remains the modality of choice when possible. The combination of MRI perfusion data with a few basic anatomic sequences,

including diffusion-weighted imaging, is the most useful tool when MRI-based decision-making is necessary in the treatment of stroke. The frequent clinical challenge is that most emergency departments are not equipped with MRI scanners. Patient transport and dependence on MRI personnel, who may need to commute to the hospital, also limit the timely acquisition of MRI data. For this reason NCCT, CT perfusion, and CTA allow a more rapid decision-making process and will likely dominate acute stroke imaging unless institutions make a concerted effort to make MRI realistically available in the acute time frame.

With DSC-MRI, rCBV and AT or TTP maps are analyzed along with anatomic and diffusion imaging. If an AIF is used to quantify the DSC data, CBF, MTT, and CBV maps are also available. In most practices, rCBV and AT or TTP maps are sufficient and easily acquired with the available software on the MRI scanner. A territory of decreased rCBV or CBV identifies infarct and can be correlated with diffusion imaging. A vascular territory of increased MTT or TTP identifies slow flow through a region of brain. There are several combinations of rCBV and TTP changes to consider. If the TTP and rCBV (or diffusion) regions of abnormality are matched, the infarct is considered complete and further intervention will likely be futile. Interestingly, studies indicate that the rCBV change is a better predictor of final infarct size than the diffusion abnormality (56). If the TTP abnormality exceeds the rCBV (or diffusion) defect, the difference represents the penumbra (Fig. 10)—the relatively hypoperfused tissue
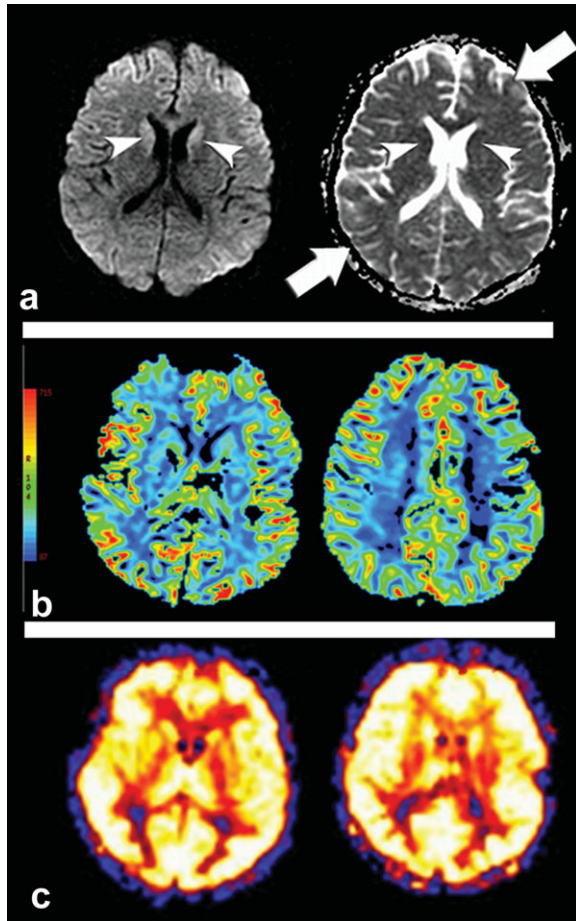
Figure 12. This young patient suffered severe trauma resulting in quadriplegia. During his prolonged hospitalization, there were multiple episodes of respiratory failure and profound hypoxia. **a:** The axial diffusion-weighted sequence and corresponding ADC map, at a glance, appear normal. There is subtle diffusion restriction in the basal ganglia (arrowheads) and possibly in the cortex of the frontal and temporoparietal lobes (arrows). **b:** Two representative images from DSC-MRI perfusion, rCBV maps. Perfusion is symmetric. Without quantification, it is difficult to comment on the global perfusion pattern. **c:** ASL perfusion CBF map demonstrates marked, globally increased perfusion to both gray matter (CBF = 163.7 mL/100g/min) and white matter, confirming the suspected clinical diagnosis of anoxic brain injury. Blood gas on the same day as this exam showed a low pCO_2 (27.9 mmHg, normal 34–45 mmHg), excluding hypercapnia as a cause of global hyperperfusion. [Color figure can be viewed in the online issue, which is available at wileyonlinelibrary.com.]

surrounding an area of infarct—which if severely hypoperfused may go on to infarct (57,58). In the event that a TTP abnormality is present yet rCBV is normal, this could be "territory at risk," a term that we reserve for perfusion disturbances with no infarct. This is distinct from penumbra, which is transit time alteration surrounding an irreversible ischemic core. These final two categories of patients, those with tissue at risk or penumbra, can potentially benefit the most from intervention. Of note, there are a variety of parameter maps that can be computed from DSC data. Measures of MTT have been found to be more associated with acute stroke clinical scores, whereas

a range of perfusion parameters have been associated with final infarct size including ATF (arrival time fitted), PTF (peak time fitted), TTP, and rMTT. Additionally, the entire concept of perfusion-diffusion mismatch is under continued investigation and refinement (59). Mismatch is a poor predictor of functional outcome (60), visual assessment of mismatch is insufficiently reliable for use in clinical trials (61), and based on several clinical trials, it is not yet clear whether penumbra determined from perfusion–diffusion mismatch benefits the selection of patients for thrombolytic therapy (62).

When considering infarct while using ASL, CBF maps are analyzed along with anatomic and diffusion imaging. Techniques for generating transit time data are in development (63,64), but are currently not routinely used with ASL. The lack of blood volume and transit time data therefore changes the interpretation of perfusion data gathered with ASL, and transit time effects may change the expected perfusion pattern in vascular disease (65). For example, in patients with very slow flow states but nonocclusive disease, the ASL tag may be suppressed in the vessels at the time of crusher gradient application and before the tag has reached the imaging plane. This may give the appearance of profound hypoperfusion or absence of perfusion, but practically, the ASL CBF map in this scenario more approximates a transit time map and, consequently, an increase in relative transit time. Furthermore, it is our experience that with concomitant DSC and ASL perfusion in patients who have suffered stroke, ASL hypoperfusion most closely associates with increases in transit time on DSC (Fig. 10). Therefore, by comparing the ASL CBF map with diffusion, some insight can be offered regarding penumbra, which manifests as an ASL hypoperfusion territory in excess of that which restricts diffusion. As with DSC-MRI, the ASL techniques can demonstrate tissue at risk as well. When a territorial hypoperfusion pattern is present on ASL without a corresponding anatomic or diffusion abnormality, we recommend vascular assessment with CTA, MRA, or, if necessary, catheter angiography, which can demonstrate significant proximal stenosis, perhaps in need of treatment (Fig. 11). Identifying such patients is just one potential benefit of routine screening perfusion sequences included with all brain MRI. With regard to determining infarct core and penumbra, it is important to keep in mind that the assumption that the DWI lesion is the core of an infarct is likely an oversimplification. Reversibility of all or part of a DWI lesion can occur following reperfusion. There is evidence that measures of MTT may provide improved infarct prediction both within and outside DWI positive lesions (66). Additionally, areas deemed to be noncore–nonpenumbral by imaging may go on to contribute to final infarct size and the associated negative clinical impact (67).

Autoregulatory disturbances can be global or focal. Regarding global disturbances in autoregulation, this is more likely to be recognized with ASL techniques given the ability to quantify CBF, whereas with DSC-MRI, one typically looks for asymmetry of the maps, which display relative data (Fig. 12). On ASL, global hyperperfusion can be seen in normal pediatric
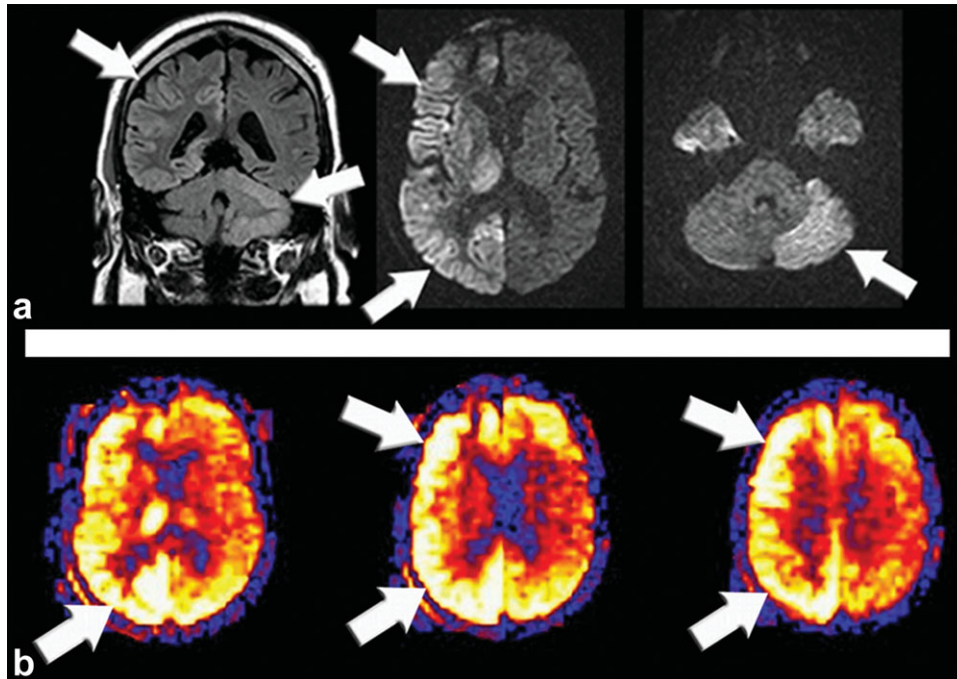
Figure 13. This 42-year-old man was found in status epilepticus of unknown duration. **a:** Coronal FLAIR (left) and axial diffusion (center, right) MRI demonstrates increased T2 signal and diffusion restriction within the right cerebral hemisphere and left cerebellar hemisphere (arrows). **b:** ASL perfusion CBF map confirms hyperperfusion within the right cerebral hemisphere (arrows). The posterior cranial fossa is not routinely imaged with our screening ASL protocol, given the limited number of slices that can be performed. Based on these findings, it was suggested that the seizures originated within the right cerebral hemisphere, resulting in cortical injury and crossed cerebellar diaschisis. Clinically, the patient recovered with no signs of cortical infarct. [Color figure can be viewed in the online issue, which is available at wileyonlinelibrary.com.]

patients, hypercapnia, and after an anoxic/hypoxic injury (34,68,69). Hemispheric hyperperfusion can be seen following carotid endarterectomy (50,70). Focal areas of hyperperfusion related to autoregulatory disturbance can also be seen. With subacute infarcts, autoregulatory dysfunction manifests as "intravascular enhancement" on postcontrast anatomic imaging (71) and focal areas of hyperperfusion on ASL (luxury perfusion), often within the deep gray structures and peripheral cortex (Fig. 3). A similar phenomenon is seen in reperfusion, resulting from spontaneous thrombolysis, thrombolytic-induced reperfusion, or anatomic bypass of previously ischemic brain tissue (32,50).

In summary, with DSC-MRI perfusion, territorially increased TTP identifies tissue with vascular perturbation. If matched by a decrease in rCBV and/or diffusion restriction, then it is considered a completed infarction. If the TTP abnormality exceeds the size of the rCBV or diffusion abnormality, penumbra is likely. If there is territorially increased TTP without accompanying rCBV or diffusion abnormality, then territory at risk for infarct is identified. Similar changes are seen with ASL, but it must be kept in mind that only CBF is calculated by ASL. However, as outlined above, in patients suffering infarct (assuming crusher gradients are used), the ASL CBF map approximates transit times. Therefore, an ASL-diffusion match can be considered to represent a completed infarct, whereas an ASL-diffusion mismatch potentially identifies penumbra. Given the ability to quantify CBF, ASL is very useful in the assessment of hyperperfusion states and autoregulatory dysfunction. When infarct is suspected or known, either the DSC or ASL method typically suffices.

Other Uses of Perfusion Imaging

Perfusion imaging has shown utility in the evaluation of epilepsy patients. There is extensive literature regarding nuclear medicine techniques when imaging potential seizure foci. Ictal SPECT relies on administering a radiopharmaceutical during seizure activity and the distribution of radiotracer equates with perfusion of the brain at ictus. Interictal SPECT or PET demonstrates relative brain perfusion between seizure episodes. It is accepted that during the ictal phase the seizure focus is relatively hyperperfused and during the interictal phase the seizure focus and surrounding tissues are relatively hypoperfused, but there is controversy as to which is more sensitive in predicting the seizure focus (72). DSC-MRI, predictably, correlates well with observations from nuclear medicine techniques—increased rCBV has been reported on ictal perfusion scans (73). Similarly, focal hyperperfusion is demonstrated in seizure foci with ASL (Fig. 13), but most successfully in supratentorial, extratemporal seizure foci (74,75). In the setting of mesial temporal sclerosis, given the proximity to the skull base and sphenoid sinus (areas which interject artifact on EPI based sequences), perfusion imaging can be more difficult (76). Regarding interictal MRI perfusion, our experience is more extensive with ASL.
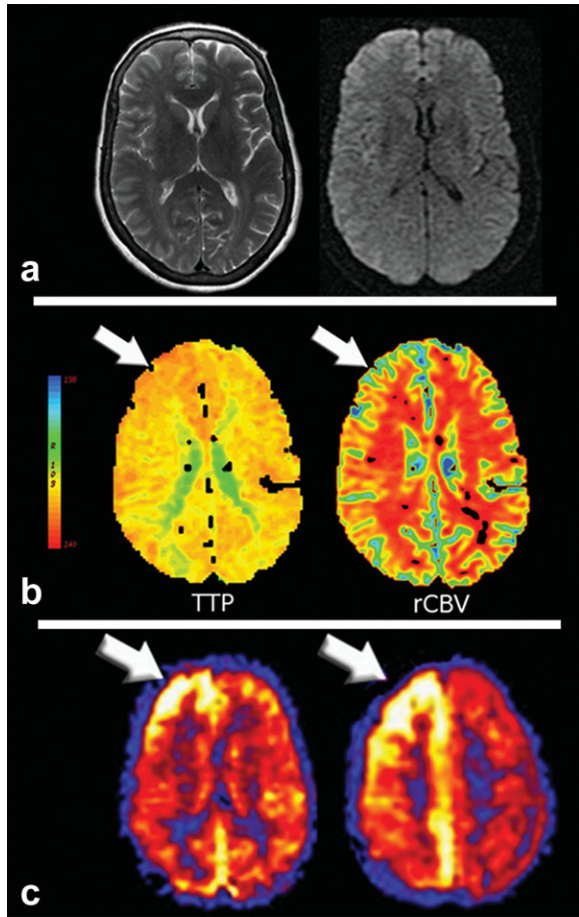
Figure 14. A patient with a history of migraine presenting with hemiplegia. **a:** Axial T2 (left) and diffusion weighted imaging (right) are normal. **b:** There is slight asymmetry on the TTP (left) and rCBV (right) maps from DSC-MRI perfusion imaging, with decreased TTP and increased rCBV (arrows) within the right hemisphere. **c:** The hyperperfusion to the right hemisphere is strikingly apparent on ASL MRI perfusion CBF maps (arrows). The differential for this pattern includes TIA with reperfusion, but this patient had no risk factors for cerebral infarct and was known to have migraines. [Color figure can be viewed in the online issue, which is available at wileyonlinelibrary.com.]

Diminished CBF on ASL in a patient with epilepsy and without risk factors for ischemia is suggestive of an interictal phase epileptogenic territory (32). Perhaps the most practical benefit of MRI perfusion in the assessment of an epilepsy population is the ability to acquire simultaneous anatomic data; for example, in assessment for mesial temporal sclerosis or neocortical epilepsies.

In the posterior reversible encephalopathy syndrome (PRES) and PRES-like syndromes, there is loss of autoregulation within the posterior circulation. This is postulated to preferentially effect the posterior circulation because of relatively fewer perivascular sympathetic nerves (77). As a result of this dysregulation, vasoconstriction occurs in an effort to maintain perfusion pressures, initially manifesting as hypoperfusion. Ultimately, rebound hyperperfusion and reversible edema ensues. In some cases, the areas of hyperperfusion may evolve into infarcts, manifesting as focal areas of hypoperfusion most commonly in the parieto-occipital lobes (32,50).

Although the exact pathophysiology of migraine headaches is not known, the vascular theory suggests that the headache is in part related to vasoconstriction (capable of generating an aura or focal neurologic deficits) followed by vasodilatation (which induces the headache) (78,79). MRI perfusion seems to support this to some degree, and because of the potential to mimic an infarct during the aura phase, migraine headaches may be imaged in this acute setting. ASL demonstrates hypoperfusion in the cortex thought to correspond to the aura symptom. However, it is more common for migraine sufferers to be imaged during the headache phase of presentation, which typically demonstrates hyperperfusion in that cortex which is thought to generate the aura (80,81). Both ASL (82) and DSC-MRI (81) have shown postaura hyperperfusion in the cortex affected by the migraine (Fig. 14). An advantage of ASL is the ability to repeat the perfusion examination without delay, which can be useful in the assessment of pathologies, like migraine, which exhibit various phases that evolve quickly (83).

CONCLUSIONS

While DSC was one of the earliest MRI perfusion techniques conceived, validated, and implemented clinically, there has been increasing interest in ASL as it gains application into major MRI vendor platforms. Neither technique is perfect, but each has its own clinical "strengths" (Table 1). In general, for screening examinations or in patients with renal failure, ASL is recommended. If a patient has received gadolinium

Table 1.
Summary of Perfusion Methods. [Color table can be viewed in the online issue, which is available at wileyonlinelibrary.com.]

Perfusion Method	TIA	Tumors	Radiation Necrosis vs Recurrent Tumor	AVM	Slow Flow	Recently Received Gadolinium	Low GFR and concern for NSF	Global Perfusion Abnormality	Perfusion Screening	Infarct	Migraine Seizure PRES
ASL	green	green	green	green	green	red	green	green	green	green	green
DSC	green	green	green	green	green	green	red	red	green	green	green
DCE	yellow	green	green	red	red	green	red	red	green	yellow	yellow

green	Best Clinical Utility/Benefit
yellow	Indeterminate Clinical Utility/Benefit
red	Limited Clinical Utility/Benefit

within the last 24 hours, DSC or DCE should be performed because the ASL signal will be destroyed by the T1 effects of the gadolinium. For global physiologic conditions, ASL is recommended. For tumors, any perfusion method can be used. For cases of tumor recurrence versus radiation necrosis, each technique can be considered. For transient ischemic attack or stroke, DSC or ASL can augment routine anatomic imaging. Emerging techniques of PCASL, ASL transit time methods, and DCE-MRI perfusion will likely further the complementary roles of the various perfusion techniques.

ACKNOWLEDGMENT

REFERENCES

1. Tofts PS. Modeling tracer kinetics in dynamic Gd-DTPA MR imaging. J Magn Reson Imaging 1997;7:91–101.
2. Rosen BR, Belliveau JW, Vevea JM, Brady TJ. Perfusion imaging with NMR contrast agents. Magn Reson Med 1990;14:249–265.
3. Edelman RR, Mattle HP, Atkinson DJ, et al. Cerebral blood flow: assessment with dynamic contrast-enhanced T2*-weighted MR imaging at 1.5 T. Radiology 1990;176:211–220.
4. Boxerman JL, Hamberg LM, Rosen BR, Weisskoff RM. MR contrast due to intravascular magnetic susceptibility perturbations. Magn Reson Med 1995;34:555–566.
5. Zierler KL. Theoretical basis of indicator-dilution methods for measuring flow and volume. Circ Res 1962;10:393–407.
6. Roberts GW, Larson KB, Spaeth EE. The interpretation of mean transit time measurements for multiphase tissue systems. J Theor Biol 1973;39:447–475.
7. Paulson ES, Schmainda KM. Comparison of dynamic susceptibility-weighted contrast-enhanced MR methods: recommendations for measuring relative cerebral blood volume in brain tumors. Radiology 2008;249:601–613.
8. Axel L. Cerebral blood flow determination by rapid-sequence computed tomography: theoretical analysis. Radiology 1980;137:679–686.
9. Cha S, Knopp EA, Johnson G, Wetzel SG, Litt AW, Zagzag D. Intracranial mass lesions: dynamic contrast-enhanced susceptibility-weighted echo-planar perfusion MR imaging. Radiology 2002;223:11–29.
10. Jackson A. Analysis of dynamic contrast enhanced MRI. Br J Radiol 2004;77(Spec No 2):S154–166.
11. Paldino MJ, Barboriak DP. Fundamentals of quantitative dynamic contrast-enhanced MR imaging. Magn Reson Imaging Clin N Am 2009;17:277–289.
12. Kjolby BF, Mikkelsen IK, Pedersen M, Ostergaard L, Kiselev VG. Analysis of partial volume effects on arterial input functions using gradient echo: a simulation study. Magn Reson Med 2009;61:1300–1309.
13. Perman WH, Gado MH, Larson KB, Perlmutter JS. Simultaneous MR acquisition of arterial and brain signal-time curves. Magn Reson Med 1992;28:74–83.
14. Rempp KA, Brix G, Wenz F, Becker CR, Guckel F, Lorenz WJ. Quantification of regional cerebral blood flow and volume with dynamic susceptibility contrast-enhanced MR imaging. Radiology 1994;193:637–641.
15. Belliveau JW, Rosen BR, Kantor HL, et al. Functional cerebral imaging by susceptibility-contrast NMR. Magn Reson Med 1990;14:538–546.
16. Hu LS, Baxter LC, Pinnaduwage DS, et al. Optimized preload leakage-correction methods to improve the diagnostic accuracy of dynamic susceptibility-weighted contrast-enhanced perfusion MR imaging in posttreatment gliomas. AJNR Am J Neuroradiol 2010;31:40–48.
17. Kiselev VG. Transverse relaxation effect of MRI contrast agents: a crucial issue for quantitative measurements of cerebral perfusion. J Magn Reson Imaging 2005;22:693–696.
18. O'Connor JP, Jackson A, Parker GJ, Jayson GC. DCE-MRI biomarkers in the clinical evaluation of antiangiogenic and vascular disrupting agents. Br J Cancer 2007;96:189–195.
19. Larsson HB, Stubgaard M, Frederiksen JL, Jensen M, Henriksen O, Paulson OB. Quantitation of blood-brain barrier defect by magnetic resonance imaging and gadolinium-DTPA in patients with multiple sclerosis and brain tumors. Magn Reson Med 1990;16:117–131.
20. Tofts PS, Kermode AG. Measurement of the blood-brain barrier permeability and leakage space using dynamic MR imaging. 1. Fundamental concepts. Magn Reson Med 1991;17:357–367.
21. Sourbron S, Ingrisch M, Siefert A, Reiser M, Herrmann K. Quantification of cerebral blood flow, cerebral blood volume, and blood-brain-barrier leakage with DCE-MRI. Magn Reson Med 2009;62:205–217.
22. Larsson HB, Courivaud F, Rostrup E, Hansen AE. Measurement of brain perfusion, blood volume, and blood-brain barrier permeability, using dynamic contrast-enhanced T(1)-weighted MRI at 3 Tesla. Magn Reson Med 2009;62:1270–1281.
23. Williams DS, Detre JA, Leigh JS, Koretsky AP. Magnetic resonance imaging of perfusion using spin inversion of arterial water. Proc Natl Acad Sci U S A 1992;89:212–216.
24. Sadowski EA, Bennett LK, Chan MR, et al. Nephrogenic systemic fibrosis: risk factors and incidence estimation. Radiology 2007;243:148–157.
25. Yang Y, Frank JA, Hou L, Ye FQ, McLaughlin AC, Duyn JH. Multislice imaging of quantitative cerebral perfusion with pulsed arterial spin labeling. Magn Reson Med 1998;39:825–832.
26. Ye FQ, Berman KF, Ellmore T, et al. H(2)(15)O PET validation of steady-state arterial spin tagging cerebral blood flow measurements in humans. Magn Reson Med 2000;44:450–456.
27. Liu TT, Brown GG. Measurement of cerebral perfusion with arterial spin labeling. Part 1. Methods. J Int Neuropsychol Soc 2007;13:517–525.
28. Zaharchuk G, Ledden PJ, Kwong KK, Reese TG, Rosen BR, Wald LL. Multislice perfusion and perfusion territory imaging in humans with separate label and image coils. Magn Reson Med 1999;41:1093–1098.
29. Dai W, Garcia D, de Bazelaire C, Alsop DC. Continuous flow-driven inversion for arterial spin labeling using pulsed radio frequency and gradient fields. Magn Reson Med 2008;60:1488–1497.
30. Wong EC, Cronin M, Wu WC, Inglis B, Frank LR, Liu TT. Velocity-selective arterial spin labeling. Magn Reson Med 2006;55:1334–1341.
31. Wu WC, Wong EC. Intravascular effect in velocity-selective arterial spin labeling: the choice of inflow time and cutoff velocity. Neuroimage 2006;32:122–128.
32. Pollock JM, Tan H, Kraft RA, Whitlow CT, Burdette JH, Maldjian JA. Arterial spin-labeled MR perfusion imaging: clinical applications. Magn Reson Imaging Clin N Am 2009;17:315–338.
33. Deibler AR, Pollock JM, Kraft RA, Tan H, Burdette JH, Maldjian JA. Arterial spin-labeling in routine clinical practice. Part 1. Technique and artifacts. AJNR Am J Neuroradiol 2008;29:1228–1234.
34. Whitlow CT, Pollock JM, Mussat-Whitlow B, et al. Changes in global rates of cerebral perfusion associated with normal development as meaured with MR arterial spin labeling. In: Am Soc Neuroradiol, 46th Annual Meeting, New Orleans; 2008.
35. Ye FQ, Frank JA, Weinberger DR, McLaughlin AC. Noise reduction in 3D perfusion imaging by attenuating the static signal in arterial spin tagging (ASSIST). Magn Reson Med 2000;44:92–100.
36. Luh WM, Wong EC, Bandettini PA, Hyde JS. QUIPSS II with thin-slice TI1 periodic saturation: a method for improving accuracy of quantitative perfusion imaging using pulsed arterial spin labeling. Magn Reson Med 1999;41:1246–1254.
37. Tan H, Maldjian JA, Pollock JM, et al. A fast, effective filtering method for improving clinical pulsed arterial spin labeling MRI. J Magn Reson Imaging 2009;29:1134–1139.
38. Maldjian JA, Laurienti PJ, Burdette JH, Kraft RA. Clinical implementation of spin-tag perfusion magnetic resonance imaging. J Comput Assist Tomogr 2008;32:403–406.
39. Kim SG, Tsekos NV. Perfusion imaging by a flow-sensitive alternating inversion recovery (FAIR) technique: application to functional brain imaging. Magn Reson Med 1997;37:425–435.
40. Leon SP, Folkerth RD, Black PM. Microvessel density is a prognostic indicator for patients with astroglial brain tumors. Cancer 1996;77:362–372.
41. Folkerth RD. Descriptive analysis and quantification of angiogenesis in human brain tumors. J Neurooncol 2000;50:165–172.
42. Folkerth RD. Histologic measures of angiogenesis in human primary brain tumors. Cancer Treat Res 2004;117:79–95.

43. Maeda M, Itoh S, Kimura H, et al. Tumor vascularity in the brain: evaluation with dynamic susceptibility-contrast MR imaging. Radiology 1993;189:233–238.

44. Aronen HJ, Gazit IE, Louis DN, et al. Cerebral blood volume maps of gliomas: comparison with tumor grade and histologic findings. Radiology 1994;191:41–51.

45. Aronen HJ, Pardo FS, Kennedy DN, et al. High microvascular blood volume is associated with high glucose uptake and tumor angiogenesis in human gliomas. Clin Cancer Res 2000;6:2189–2200.

46. Law M, Yang S, Wang H, et al. Glioma grading: sensitivity, specificity, and predictive values of perfusion MR imaging and proton MR spectroscopic imaging compared with conventional MR imaging. AJNR Am J Neuroradiol 2003;24:1989–1998.

47. Brown GG, Clark C, Liu TT. Measurement of cerebral perfusion with arterial spin labeling. Part 2. Applications. J Int Neuropsychol Soc 2007;13:526–538.

48. Kim HS, Kim SY. A prospective study on the added value of pulsed arterial spin-labeling and apparent diffusion coefficients in the grading of gliomas. AJNR Am J Neuroradiol 2007;28:1693–1699.

49. Jarnum H, Steffensen EG, Knutsson L, et al. Perfusion MRI of brain tumours: a comparative study of pseudo-continuous arterial spin labelling and dynamic susceptibility contrast imaging. Neuroradiology 2010;52:307–317.

50. Deibler AR, Pollock JM, Kraft RA, Tan H, Burdette JH, Maldjian JA. Arterial spin-labeling in routine clinical practice. Part 3. Hyperperfusion patterns. AJNR Am J Neuroradiol 2008;29:1428–1435.

51. Lev MH, Ozsunar Y, Henson JW, et al. Glial tumor grading and outcome prediction using dynamic spin-echo MR susceptibility mapping compared with conventional contrast-enhanced MR: confounding effect of elevated rCBV of oligodendrogliomas [corrected]. AJNR Am J Neuroradiol 2004;25:214–221.

52. Meyzer C, Dhermain F, Ducreux D, et al. A case report of pseudo-progression followed by complete remission after proton-beam irradiation for a low-grade glioma in a teenager: the value of dynamic contrast-enhanced MRI. Radiat Oncol 2010;5:9.

53. Gahramanov S, Raslan AM, Muldoon LL, et al. Potential for differentiation of pseudoprogression from true tumor progression with dynamic susceptibility-weighted contrast-enhanced magnetic resonance imaging using ferumoxytol vs. gadoteridol: a pilot study. Int J Radiat Oncol Biol Phys 2011;79:514–523.

54. Tanaka Y, Nagaoka T, Nair G, Ohno K, Duong TQ. Arterial spin labeling and dynamic susceptibility contrast CBF MRI in post-ischemic hyperperfusion, hypercapnia, and after mannitol injection. J Cereb Blood Flow Metab 2011;31:1403–1411.

55. Ernst TM, Chang L, Witt MD, et al. Cerebral toxoplasmosis and lymphoma in AIDS: perfusion MR imaging experience in 13 patients. Radiology 1998;208:663–669.

56. Karonen JO, Vanninen RL, Liu Y, et al. Combined diffusion and perfusion MRI with correlation to single-photon emission CT in acute ischemic stroke. Ischemic penumbra predicts infarct growth. Stroke 1999;30:1583–1590.

57. Ueda T, Yuh WT, Maley JE, Quets JP, Hahn PY, Magnotta VA. Outcome of acute ischemic lesions evaluated by diffusion and perfusion MR imaging. AJNR Am J Neuroradiol 1999;20:983–989.

58. Neumann-Haefelin T, Wittsack HJ, Wenserski F, et al. Diffusion- and perfusion-weighted MRI. The DWI/PWI mismatch region in acute stroke. Stroke 1999;30:1591–1597.

59. Kane I, Carpenter T, Chappell F, et al. Comparison of 10 different magnetic resonance perfusion imaging processing methods in acute ischemic stroke: effect on lesion size, proportion of patients with diffusion/perfusion mismatch, clinical scores, and radiologic outcomes. Stroke 2007;38:3158–3164.

60. Kane I, Hand PJ, Rivers C, et al. A practical assessment of magnetic resonance diffusion-perfusion mismatch in acute stroke: observer variation and outcome. J Neurol 2009;256:1832–1838.

61. Campbell BC, Christensen S, Foster SJ, et al. Visual assessment of perfusion-diffusion mismatch is inadequate to select patients for thrombolysis. Cerebrovasc Dis 2010;29:592–596.

62. Wechsler LR. Imaging evaluation of acute ischemic stroke. Stroke 2011;42(1 Suppl):S12–15.

63. Wang J, Alsop DC, Song HK, et al. Arterial transit time imaging with flow encoding arterial spin tagging (FEAST). Magn Reson Med 2003;50:599–607.

64. Barbier EL, Silva AC, Kim SG, Koretsky AP. Perfusion imaging using dynamic arterial spin labeling (DASL). Magn Reson Med 2001;45:1021–1029.

65. Deibler AR, Pollock JM, Kraft RA, Tan H, Burdette JH, Maldjian JA. Arterial spin-labeling in routine clinical practice, part 2: hypoperfusion patterns. AJNR Am J Neuroradiol 2008;29:1235–1241.

66. Carrera E, Jones PS, Alawneh JA, et al. Predicting infarction within the diffusion-weighted imaging lesion: does the mean transit time have added value? Stroke 2011;42:1602–1607.

67. Alawneh JA, Jones PS, Mikkelsen IK, et al. Infarction of 'non-core-non-penumbral' tissue after stroke: multivariate modelling of clinical impact. Brain 2011;134(Pt 6):1765–1776.

68. Pollock JM, Deibler AR, Whitlow CT, et al. Hypercapnia-induced cerebral hyperperfusion: an underrecognized clinical entity. AJNR Am J Neuroradiol 2009;30:378–385.

69. Pollock JM, Whitlow CT, Deibler AR, et al. Anoxic injury-associated cerebral hyperperfusion identified with arterial spin-labeled MR imaging. AJNR Am J Neuroradiol 2008;29:1302–1307.

70. Wagner WH, Cossman DV, Farber A, Levin PM, Cohen JL. Hyperperfusion syndrome after carotid endarterectomy. Ann Vasc Surg 2005;19:479–486.

71. Elster AD, Moody DM. Early cerebral infarction: gadopentetate dimeglumine enhancement. Radiology 1990;177:627–632.

72. Oommen KJ, Saba S, Oommen JA, Francel PC, Arnold CD, Wilson DA. The relative localizing value of interictal and immediate postictal SPECT in seizures of temporal lobe origin. J Nucl Med 2004;45:2021–2025.

73. Warach S, Levin JM, Schomer DL, Holman BL, Edelman RR. Hyperperfusion of ictal seizure focus demonstrated by MR perfusion imaging. AJNR Am J Neuroradiol 1994;15:965–968.

74. Wolf RL, Alsop DC, Levy-Reis I, et al. Detection of mesial temporal lobe hypoperfusion in patients with temporal lobe epilepsy by use of arterial spin labeled perfusion MR imaging. AJNR Am J Neuroradiol 2001;22:1334–1341.

75. Pollock JM, Deibler AR, West TG, Burdette JH, Kraft RA, Maldjian JA. Arterial spin-labeled magnetic resonance imaging in hyperperfused seizure focus: a case report. J Comput Assist Tomogr 2008;32:291–292.

76. Engelhorn T, Doerfler A, Weise J, Baehr M, Forsting M, Hufnagel A. Cerebral perfusion alterations during the acute phase of experimental generalized status epilepticus: prediction of survival by using perfusion-weighted MR imaging and histopathology. AJNR Am J Neuroradiol 2005;26:1563–1570.

77. Casey SO, McKinney A, Teksam M, Liu H, Truwit CL. CT perfusion imaging in the management of posterior reversible encephalopathy. Neuroradiology 2004;46:272–276.

78. Wolff HG, Marcussen RM, Kunkle EC. Studies on headache; analysis of the contractile state of the cranial vascular tree in migraine. Trans Am Neurol Assoc 1948;73:14–17.

79. Oberndorfer S, Wober C, Nasel C, et al. Familial hemiplegic migraine: follow-up findings of diffusion-weighted magnetic resonance imaging (MRI), perfusion-MRI and [99mTc] HMPAO-SPECT in a patient with prolonged hemiplegic aura. Cephalalgia 2004;24:533–539.

80. Goadsby PJ. Migraine pathophysiology. Headache 2005;45(Suppl 1):S14–24.

81. Jacob A, Mahavish K, Bowden A, Smith ET, Enevoldson P, White RP. Imaging abnormalities in sporadic hemiplegic migraine on conventional MRI, diffusion and perfusion MRI and MRS. Cephalalgia 2006;26:1004–1009.

82. Pollock JM, Deibler AR, Burdette JH, et al. Migraine associated cerebral hyperperfusion with arterial spin-labeled MR imaging. AJNR Am J Neuroradiol 2008;29:1494–1497.

83. Kato Y, Araki N, Matsuda H, Ito Y, Suzuki C. Arterial spin-labeled MRI study of migraine attacks treated with rizatriptan. J Headache Pain 2010;11:255–258.